Exact-enumeration approach to multifractal structure for diffusion-limited aggregation

Jysoo Lee, Preben Alstrøm, and H. Eugene Stanley
Center for Polymer Studies and Department of Physics, Boston University, Boston, Massachusetts 02215
(Received 27 December 1988)

Using an exact-enumeration approach, we study the multifractal spectrum of diffusion-limited aggregation. The enormous number of possible configurations is reduced by many orders of magnitude using symmetry considerations. The most interesting result is that we find evidence which strongly suggests the existence of a phase transition in the multifractal spectrum: specifically, the "free energy," "energy," and "specific heat" develop singularities near a critical "temperature" β_c. Moreover, the energy shows large fluctuations near β_c. We also find that for $\beta<\beta_c$, the free energy is dominated by the maximum energy $E_{\max}(L)$, which increases with system size L: $E_{\max}(L)\sim L^2/\ln L$. The implications of this phase transition are that the free energy is not defined for $\beta<\beta_c$, and that the large energy part of the "entropy" function is a straight line of slope β_c. We provide a phenomenological explanation for the origin of this phase transition.

I. INTRODUCTION

The diffusion-limited aggregation[1] (DLA) model has been found to describe a remarkably large number of interesting physical systems such as fluid flow in porous media, colloidal aggregation, and electrodeposition.[2–17] Although DLA is one of the most important models of fractal growth phenomena, and is described by a quite simple set of rules, there has been surprisingly little understanding of this model. For example, even the existence of the fractal dimension in the large-cluster limit is not clear. The situation becomes more complicated, since the fractal dimension alone is not sufficient to characterize the growth process.[4–6] Furthermore, in order to *fully* characterize the growth process, one needs an infinite number of independent exponents, which is usually called the multifractal spectrum.[7–9]

There have been enormous efforts to calculate the multifractal spectrum of DLA using various techniques such as real-space renormalization,[10] numerical simulations,[5,6,13] phenomenological arguments,[11,14] conformal mapping,[15–16] fixed-scale transformation,[17] and a field-theoretical method.[12] Owing to these efforts, valuable information for some part of the spectrum has been obtained. Especially for the region corresponding to the "tip" of the cluster, most of the methods seem to give similar results. However, the exact solution for the multifractal spectrum has not been determined at present.

In particular, there has been essentially no reliable information for the part of the spectrum corresponding to the "fjord" of the DLA cluster. The origin of this difficulty is the fact that this region is characterized by *extremely* small growth probabilities. Therefore, numerical simulation cannot give reliable results due to numerical accuracy (the smallest growth probability for a large DLA cluster is much smaller than the numerical accuracy). Furthermore, different methods seem to give different results and also disagree with the experiments, a fact that has plagued investigators in this field.[18]

In this paper, we study the multifractal spectrum of DLA based on an exact enumeration approach, which means we *must* consider every possible cluster configuration up to a certain size. This exact enumeration follows the general procedure outlined by Nagatani[19] in connection with a position-space renormalization-group formulation for DLA. Since we find the minimum growth probability to a high numerical accuracy, we can determine the fjord part of the multifractal spectrum.

We consider clusters of size L, where $L=2,3,4,5$. We find out that we have to consider 3.0×10^{17} different cluster configurations for $L=5$. By finding symmetries in the system, we are able to reduce them to 9361 configurations, which indicates there are enormous numbers of symmetries in the system.

Furthermore, we find evidence suggesting the existence of a phase transition[20,21] in the multifractal spectrum. In other words, the "free energy" of the system develops a singularity near a certain critical "temperature." We also find that this transition has several interesting consequences. For example, the free energy is not defined below the critical temperature β_c, the large energy part of the "entropy" function is a straight line of slope β_c, and there are large fluctuations of energy near the critical temperature. We also give a phenomenological explanation for the origin of this phase transition.[22]

This paper is organized as follows. In Sec. II, we describe the exact enumeration method used here to obtain the multifractal spectrum. The method which reduces the number of independent configurations based on symmetry considerations is given in Sec. III. In Sec. IV, we describe the evidence of a phase transition and its consequences. The origin of a phase transition is explained using a phenomenological argument in Sec. V. The summary and open questions can be found in Sec. VI.

II. EXACT ENUMERATION METHOD

In this section, we will describe the method used here to obtain the multifractal spectrum. Consider the dielectric breakdown model[23] (DBM), which has the same

mathematical structure as DLA. For DBM, one solves the Laplace equation for the electrical potential ϕ, with boundary conditions $\phi=1$ on the cluster and $\phi=0$ at infinity. In this paper, we will consider DBM in the strip geometry; here one replaces the point seed with a line of seed particles, and one chooses $\phi=1$ for all particles connected to this line and $\phi=0$ for points an infinite distance above the cluster. It is believed that the fractal properties of the original DBM problem with circular geometry are the same as those for the DBM in the strip geometry. Furthermore, we shall take periodic boundary conditions in the horizontal direction, so that our strip is effectively wrapped onto a cylinder.

The first step is to consider a finite lattice of edge L. Every bond can be considered to be a resistor. If we assign an infinite conductance to the bonds belonging to the cluster, and unit conductance for the other bonds, with the boundary conditions $\phi=1$ on the cluster and $\phi=0$ along the top of the lattice, then this resistor network problem becomes equivalent to DBM in the $L\rightarrow\infty$ limit. Since the resistor network is more convenient than DBM for small-cell exact enumeration, we will mostly consider the resistor network problems henceforth.

We use a finite-cell exact-enumeration method to study the scaling structure of DLA. This means we must consider *every possible configuration* for a given cell size. Furthermore, we use a renormalization method developed by Nagatani.[19] The basic idea of his method is as follows. In a coarse-graining process, there is a length scale a defined as a lattice constant. The structures whose length scale is less than a are usually ignored in the process of coarse graining. For example, consider a coarse graining of a 4×4 cell configuration to a 2×2 cell, shown in Fig. 1. The solid lines are "cluster" bonds with infinite conductance. Notice that cluster bonds whose size is less than a are ignored in process 1 (marked as 2 and 4). On the other hand, cluster bonds whose size is larger than a are preserved (marked as 1).

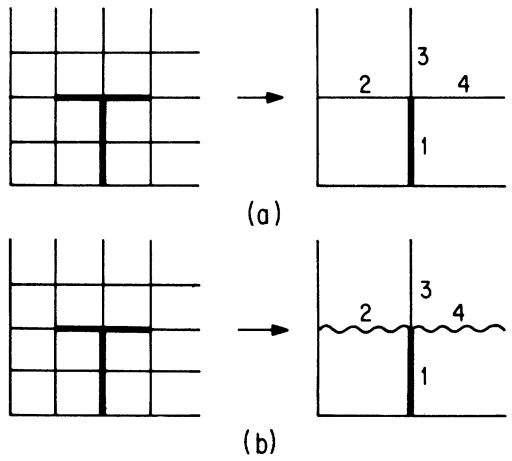

FIG. 1. Comparison of two coarse-graining processes. (a) Process 1: small structures, whose size is less than a, are ignored. (b) Process 2: small structures are replaced by bonds of effective conductance σ^*.

Instead of ignoring these small structures, one can assign an effective conductance σ^* for the bonds containing the small structures like 2,4 (process 2). Since those types of bonds are always at the tip of cluster bonds, we call them "surface" bonds. One way to calculate σ^* has been developed by Nagatani using an approximate renormalization method (see Appendix A).

Based on the above remarks, we can exactly specify the system to be studied. We cover the space with a $L\times L$ square resistor network. The conductances of the bonds (resistors) are defined as follows.

(1) If a bond is a part of the cluster, we call it a *cluster bond.* Since the potential on the cluster remains the same ($\phi=1$), we assign an infinite conductance to cluster bonds.

(2) If a bond is not a cluster bond, but one of its two ends is touching a cluster bond, it is a *surface bond.* The conductance σ^* assigned to surface bonds is calculated using a renormalization method (see Appendix A).

(3) All the other bonds are designated as *empty bonds* and assigned to a conductance of 1. Finally, we assign boundary conditions, which are $\phi=0$ at the top of the cell and $\phi=1$ at the bottom of the cell. We also apply periodic boundary conditions in a horizontal direction. A typical configuration with boundary conditions is shown in Fig. 2.

The next question to be answered is "What are the possible configurations and their weights?" Let C_α be the weight of configuration α, the probability of getting configuration α, if we randomly choose one configuration of the total possible configurations. Obviously not every combination of the three types of bonds (cluster, surface, and empty) is possible. The possible configurations and their weights are determined by the growth rule of DBM.

Consider the 2×2 case as an example. All the possible configurations and their weights are shown in Fig. 3. We start with a configuration with no cluster bonds, configuration 1, shown at the top of Fig. 3. The weight of this configuration is C_1, which will now be calculated. Note that only surface bonds can grow to be cluster bonds, since if empty bonds grow to be cluster bonds, we would have more than one cluster, and the cluster bonds cannot grow any more. The growth probability for each of the N_α surface bonds in configuration α is given by

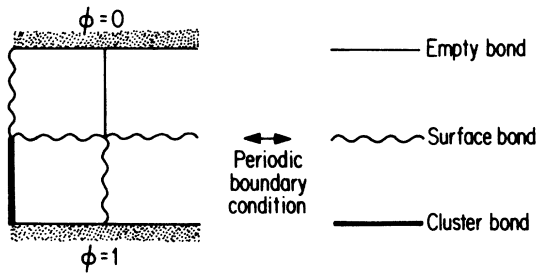

FIG. 2. A typical configuration ($L=2$ case), its boundary conditions, and three types of bonds are shown.

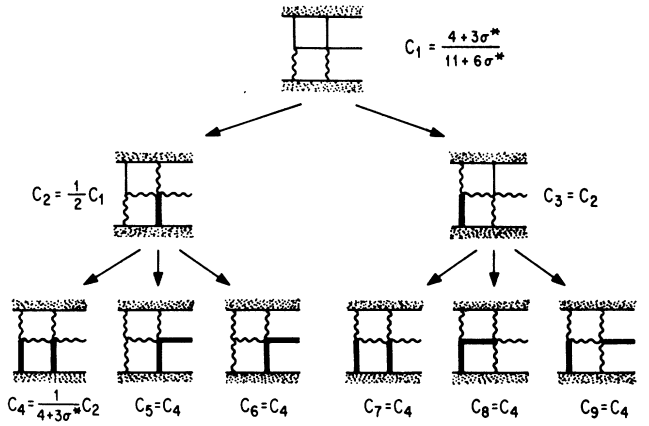

FIG. 3. All the possible configurations with their weights for the $L=2$ case.

$$p_i = \frac{(\nabla\phi)_i}{\sum_{i=1}^{N_\alpha} (\nabla\phi)_i} , \tag{1}$$

where $(\nabla\phi)_i$ is the voltage drop across the ith surface bond. For configuration 1, $N_1=2$ and $p_1=p_2=\frac{1}{2}$. Each of the surface bonds can grow and generate configurations 2 and 3 (as shown at the middle of Fig. 3). The weights of these configurations C_2, C_3 are just $p_1 C_1$ and $p_2 C_1$, respectively. We continue this growth process until all the surface bonds are grown. But we do not consider configurations which the bonds at the top vertical layers are grown, since the growth probabilities of the surface bonds in these configurations are zero. We thus determine all the possible configurations and weights as a function of C_1. C_1 can be determined from the normalization condition

$$\sum_{\alpha=1}^{N} C_\alpha = 1 , \tag{2}$$

where N is the total number of possible configurations. For the 2×2 case, $N=9$.

Since we obtained all the possible configurations and their weights, we can study the scaling structure of the growth site probability distribution using the thermodynamic formalism.[24] The "partition function" $Z(\beta,L)$ of the system is defined as

$$Z(\beta,L) \equiv \sum_{\alpha=1}^{N} C_\alpha \sum_{i=1}^{N_\alpha} p_{i,\alpha}^{\beta} , \tag{3}$$

where $p_{i,\alpha}$ is the growth probability at site i of configuration α. Motivated from the formal similarity of $Z(\beta,L)$ to the partition function of canonical ensemble, we define "free energy" as (Table I)

$$F(\beta,L) \equiv -\frac{\ln Z(\beta,L)}{\ln L} . \tag{4}$$

Furthermore, we can define the "energy" $E(\beta,L)$ and

TABLE I. Comparison of notation of this paper and that of Refs. 7–9.

This work	Refs. 7–9
$\beta \leftrightarrow q$	$F(\beta) \leftrightarrow \tau(q)$
$E \leftrightarrow \alpha$	$S(E) \leftrightarrow f(\alpha)$

"specific heat" $C(\beta,L)$ of the system,

$$E(\beta,L) \equiv \frac{\partial F(\beta,L)}{\partial \beta} , \tag{5}$$

and

$$C(\beta,L) \equiv -\frac{\partial E(\beta,L)}{\partial \beta} . \tag{6}$$

III. SYMMETRY CONSIDERATIONS

In this section, we will describe the method to reduce the complicated tree structures, such as Fig. 3 to simpler forms, based on symmetry considerations. Consider Fig. 3 more carefully. The configuration C_2 is the translation of the C_3 in the horizontal direction by one lattice constant. Furthermore, every configuration grown from C_2 (i.e., C_4, C_5, and C_6) can be obtained by translating corresponding configuration grown from C_3 (i.e., C_7, C_8, and C_9). In other words, by translating C_3 (and its daughters) in the horizontal direction by one lattice constant, we get C_2 (and its daughters). Therefore for any arbitrary configuration α from C_2 (and its daughters), one can find a corresponding configuration α' from C_3 (and its daughters), which is the translation of configuration α in horizontal direction by one lattice constant. Since the translation of a configuration in the horizontal direction leaves all the p_i invariant, α and α' must have the same p_i. Furthermore, since the weight of a configuration depends only on the ancestors and the p_i of the ancestors, C_α and $C_{\alpha'}$ should be the same.

If an operation on configuration α leaves C_α and p_i of itself and its daughters unchanged, we call the operation

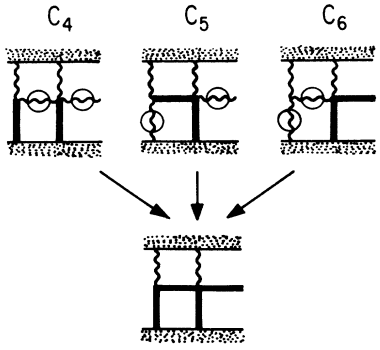

FIG. 4. Three different configurations (C_4, C_5, and C_6) become identical after replacing their zero-voltage-drop surface bonds (marked by circles) with the cluster bonds.

as *symmetry operation*. For example, translation in horizontal direction by one lattice constant is a symmetry operation.

Since p_i and C_α are the only quantities used in the evaluation of the partition function $Z(\beta,L)$, C_2 (and its daughters) and C_3 (and its daughters) make the same contribution to $Z(\beta,L)$. Therefore, instead of considering two separate branch structures, we can consider only one branch with symmetry factor 2.

In order to reduce the tree structure more, consider the three configurations at the bottom (C_4, C_5, and C_6). As shown in Fig. 4, these configurations have surface bonds which have no voltage drop across them. Let us replace these bonds with the cluster bonds. Since these bonds have zero-voltage drop, these bonds do not contribute to $Z(\beta,L)$. Furthermore, since the p_i of these bonds are zero, this replacement does not change the daughters' structures too. After the replacement, the three configurations (C_4, C_5, and C_6) become the same. So instead of considering three different branches, we can consider only one branch with symmetry factor 3. The reduced tree structure with symmetry is shown in Fig. 5.

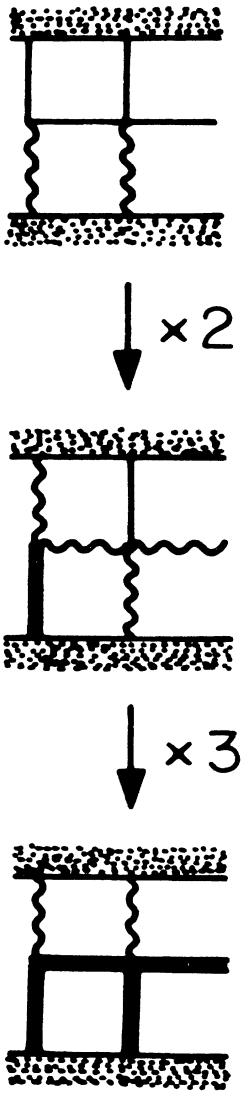

FIG. 5. All the possible configurations, with their weights, simplified by the symmetry considerations.

These symmetry considerations get more difficult as the size of the cell increases, and become practically impossible for cells with $L \geq 4$. One has to rely on the computer after that. In order to make a more efficient algorithm, we have found additional symmetry operations. Consider the inversion of a configuration around one of its vertical axes. By following the same argument for the translation, one can show that the inversion is a symmetry operation. Let I_y denote inversion operator around the yth vertical axis. Then there will be L inversion operators ($y = 1,2,\ldots,L$). If we call T_x the translation operator in the horizontal direction by the x lattice constant, there also will be L translation operators ($x = 1,2,\ldots,L$). One can notice that any operator defined as products of one of these $2L$ symmetry operators is also symmetric. However, we find that these new operators are equal to one of the $2L$ independent symmetry operators, which we choose to be $T_0, T_1, \ldots, T_{L-1}$ and $I_1, I_2, \ldots, I_L$. Two typical types of symmetric operators are shown in Fig. 6.

The other thing we have considered is the replacement of zero-voltage-drop surface bonds with cluster bonds. Although this replacement does not change the value $Z(\beta,L)$, as argued before, it gives us two very important advantages.

The first advantage is that it reveals "hidden" symmetry. As illustrated in Fig. 4, there are configurations which can be related to each other by symmetry operations, but their identification is difficult due to zero-voltage-drop surface bonds. By this replacement, we change the configuration into "standard" form, in which the identification of symmetry is much easier.

The other advantage is that it removes unnecessary

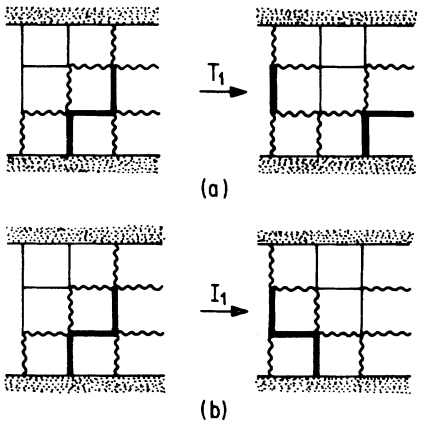

FIG. 6. Two types of symmetry operators. (a) Translational operator translates a configuration by one lattice constant in the horizontal direction. (b) Inversion operator inverts a configuration around the first vertical axis.

daughter structures. Since zero-voltage-drop surface bonds have zero growth probabilities, the daughters obtained by growing these bonds make no contribution to $Z(\beta,L)$. These unnecessary daughter structures, if not removed, use a lot of CPU time. In our calculation, we find this replacement is crucial to get results within a reasonable time.

Then, how can the computer identify these zero-voltage-drop surface bonds? One possibility is to numerically solve the Laplace equation and find the surface bonds whose voltage drops are less than a specified error. This method has two disadvantages. In order to determine the voltage distribution accurately, one needs a lot of computation time. Furthermore, there is a possibility of "misjudging" due to numerical accuracy. Instead, we use a modified version of the "burning" algorithm[25] to identify them (for more details see Appendix B).

Based on the above discussion, we constructed algorithms that produce a "reduced tree structure." With this program, we obtain the reduced tree structure up to $L=5$. In order to get an idea about the importance of the symmetries, we also calculated the number of configurations both in the original and reduced tree structures. We find that there are 9, 5323, 1.2×10^9, and 3.0×10^{17} configurations in the original tree structures for $L=2$, 3, 4, and 5, respectively. The corresponding numbers of configurations in the reduced tree structures are 3, 14, 259, and 9361, which indicates there are enormous symmetries in the system. The reason for this remarkable reduction is that we can apply the symmetry operations repeatedly. Thus, although there are only $2L$ symmetry operations, the reduction for the case $L=5$ is a factor of roughly 10^{14}.

IV. PHASE TRANSITION ON DLA

In this section, we will describe the evidence suggesting the existence of a phase transition in the multifractal spectrum of DLA, and its connection to the "negative moment problem." To be precise, consider the partition function $Z(\beta,L)$ defined in (3). The dependence of $\ln Z(\beta,L)$ on $\ln L$ for several values of β is shown in Fig. 7. For $\beta\geq0$, the data form an almost perfect straight line, which strongly suggests power-law scaling behavior of $Z(\beta,L)$. However, as β is decreased, the data begin to deviate from a straight line. Moreover, as β is decreased further, the data seem to approach an exponential curve. This suggests that the moments $Z(\beta,L)$ *do not* scale as a power law for sufficiently negative β. This deviation from power-law scaling behavior, which appears in other systems,[21] is called the "negative-moment problem." We shall argue that this negative-moment problem is a consequence of a phase transition.

To explain what we mean by a phase transition, consider the free energy $F(\beta,L)$, determined for different L values, shown in Fig. 8. One can see there are "knees" around $\beta\simeq-1$, and they get sharper as we increase the size of the system L. To see this phenomenon more clearly, we also plot the $E(\beta,L)$ curves, shown in Fig. 9.

Figure 9 shows the large change in the energy of the system for $-2\leq\beta\leq0$. Furthermore, for $\beta<-2$, $E(\beta,L)$

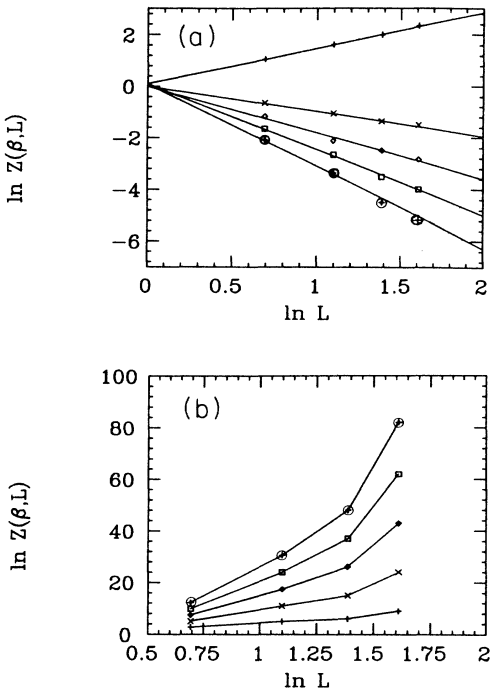

FIG. 7. Dependence of $\ln Z(\beta,L)$ on $\ln L$. (a) $\beta\geq0$, (+), (×), (◇), (□), and (⊕) means $\beta=0$, 2, 3, 4, and 5, respectively. The data form an almost perfect straight line. (b) $\beta\leq0$, (+), (×), (◇), (□), and (⊕) means $\beta=-1$, -2, -3, -4, and -5, respectively. The data deviate from a straight line as β is decreased.

becomes almost constant and is given by the maximum energy of the system $E_{\max}(L)$. The size dependence of $E_{\max}(L)$ on L is determined from the analysis of Fig. 10,

$$E_{\max}(L)\sim L^2/\ln L \ . \tag{7}$$

Next, we plot the specific heat $C(\beta,L)$ as shown in Fig. 11. One can clearly see that the maximum of $C(\beta,L)$ increases as we increase the size of the system. On the oth-

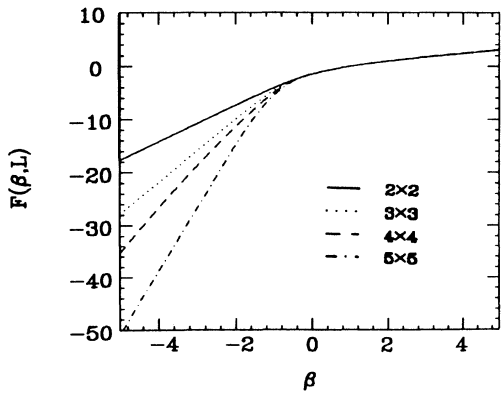

FIG. 8. Dependence of $F(\beta,L)$ on β for $L=2\sim5$. One can notice the "knees" developing around $\beta\simeq-1$.

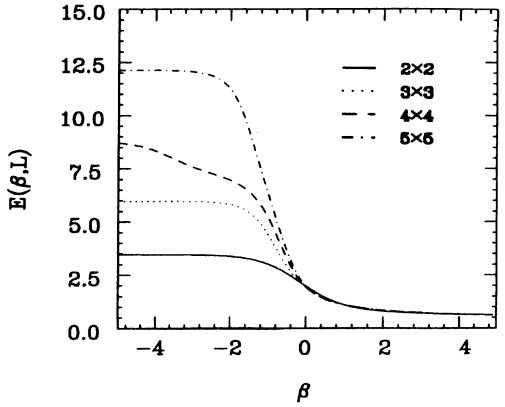

FIG. 9. Dependence of $E(\beta,L)$ on β for $L=2\sim5$. One can notice the sharp change for $-2\leq\beta\leq0$.

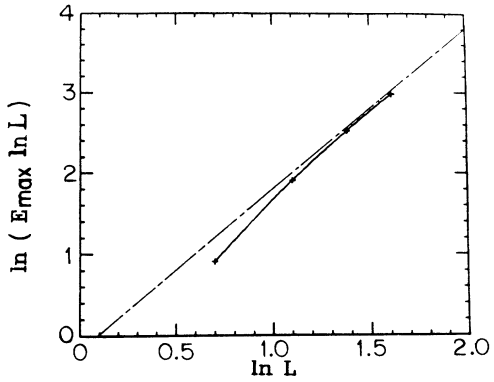

FIG. 10. Determination of L dependence of $E_{\max}(L)$. The data approach the line of slope 2 (dashed line).

er hand, $\beta_{\max}$, the temperature of the maximum $C(\beta,L)$, seems to be independent of L. Based on the above observation, we propose the following.

(1) The energy $E(\beta,L)$ shows a sharp transition around the critical temperature $\beta_c(L)$.

(2) As L is increased, the range of β in which the transition can be seen is getting smaller, and approaches a single value β_c for $L\rightarrow\infty$.

(3) Below $\beta_c(L)$, $E(\beta,L)$ jumps to the maximum energy of the system $E_{\max}(L)$ whose L dependence is given by (7).

Although these proposals cannot be proved rigorously, we will give some physical arguments supporting them in Sec. V. In the remainder of this section, we will concentrate on the consequences of this transition for the other thermodynamic quantities such as free energy and entropy function.

Then, what we can say about $F(\beta)$, which is defined as $L\rightarrow\infty$ limit of $F(\beta,L)$? For $\beta>\beta_c$, because $E(\beta)$ is a smooth curve, we expect $F(\beta)$ to be also a smooth function of β. On the other hand, for $\beta<\beta_c$, $E(\beta,L)$ equals $E_{\max}(L)$; therefore, $F(\beta,L)$ is a straight line of slope $E_{\max}(L)$. Furthermore, since $E_{\max}(L)$ diverges as $L\rightarrow\infty$, $F(\beta)$ diverges to negative infinity. This divergence of $F(\beta)$ for any $\beta<\beta_c$ is precisely the negative-moment problem stated previously. Therefore, we argue that the negative moment problem, which has plagued investigator in this field, is just a *consequence of this transition*. Moreover, since this transition implied a singularity in the free-energy function, we call it a "phase transition."

Next, consider the "entropy" function $S(E,L)$, defined as the negative of the Legendre transform of $F(\beta,L)$ with respect to the variable β,

$$S(E,L)\equiv\beta E-F(\beta,L)\ . \tag{8}$$

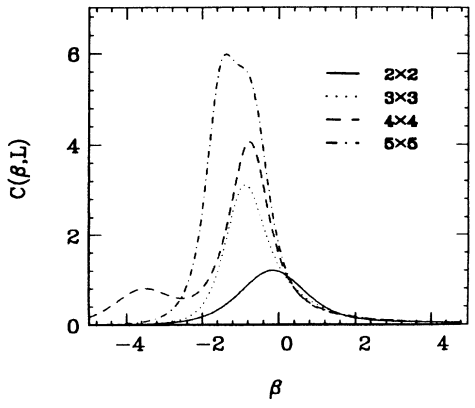

FIG. 11. Dependence of $C(\beta,L)$ on β determined for $L=2\sim5$. One can notice that the maximum value of the specific heat increases as L increases. On the other hand, their position seems to be insensitive to L.

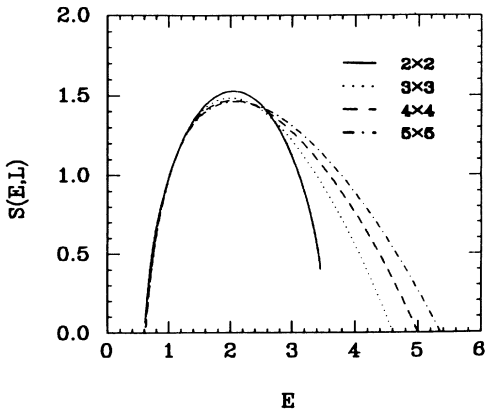

FIG. 12. Dependence of $S(E,L)$ on E determined for $L=2\sim5$. The left part shows good convergence. On the other hand, the right part is poorly convergent.

We also define $S(E)$ as the $L \to \infty$ limit of $S(E,L)$. $S(E,L)$, determined for several different L, is shown in Fig. 12. The left-hand part of $S(E,L)$, which corresponds to the $\beta \geq 0$ part of $F(\beta,L)$, shows very good convergence. On the other hand, the right-hand part of $S(E,L)$ shows poor convergence. In order to find out the meaning of this poor convergence, consider the form of $S(E)$, determined from $F(\beta)$. The $\beta > \beta_c$ part of $F(\beta)$ is mapped into the $E < E_c$ part of $S(E)$, which is expected to be a smooth function of E [where $E_c \equiv \lim_{\beta \to \beta_c^+} F'(\beta)$]. However, the $\beta = \beta_c$ part of $F(\beta)$ (a point) is mapped into a straight line of slope β_c, which is the $E \geq E_c$ part of $S(E)$. The poorly convergent part of $S(E)$ precisely corresponds to the $\beta \sim \beta_c$ part of $F(\beta)$, which is expected to converge to a straight line of slope β_c.

We next argue that this poor convergence is due to the large fluctuation of energy near β_c. In order to show this, let us first define the density of states function

$$D(\epsilon,L)d\epsilon \equiv \text{average number of surface bonds satisfying } \epsilon \leq \epsilon' \leq \epsilon + d\epsilon \ , \quad (9)$$

where $\epsilon' \equiv -\ln p / \ln L$ and p is the growth probability of the surface bonds. Furthermore, we define $s(\epsilon,L) \equiv \ln D(\epsilon,L)/\ln L$. Then the partition function can be written as

$$Z(\beta,L) = \sum_{\epsilon} D(\epsilon,L) L^{-\beta\epsilon} d\epsilon = \sum_{\epsilon} L^{s(\epsilon,L)} L^{-\beta\epsilon} d\epsilon \ . \quad (10)$$

The ϵ dependence of the function $D(\epsilon,L)L^{-\beta\epsilon}$ shows the relative contribution of different ϵ terms to $Z(\beta,L)$. The $L = 5$ case is shown in Fig. 13 for three different values of β. For β away from β_c, one can see that this function has a sharp peak near a certain value ϵ^*, which means that the ϵ^* term gives the dominant contribution to $Z(\beta,L)$, and the other contribution can be ignored. However, for $\beta \simeq \beta_c$, there seems to be no single dominant contribution, and one can see the large fluctuation of energies. This large fluctuation of energy also supports the existence of a phase transition. Because we find contributions from all energy scales for $\beta \sim \beta_c$, the derivation of $S(E,L)$ from $F(\beta,L)$ must be called into question. This derivation uses the method of steepest descent, which assumes that most of the contribution to $Z(\beta,L)$ comes from energies close to the saddle-point energy ϵ^*. In this case, $S(E,L)$

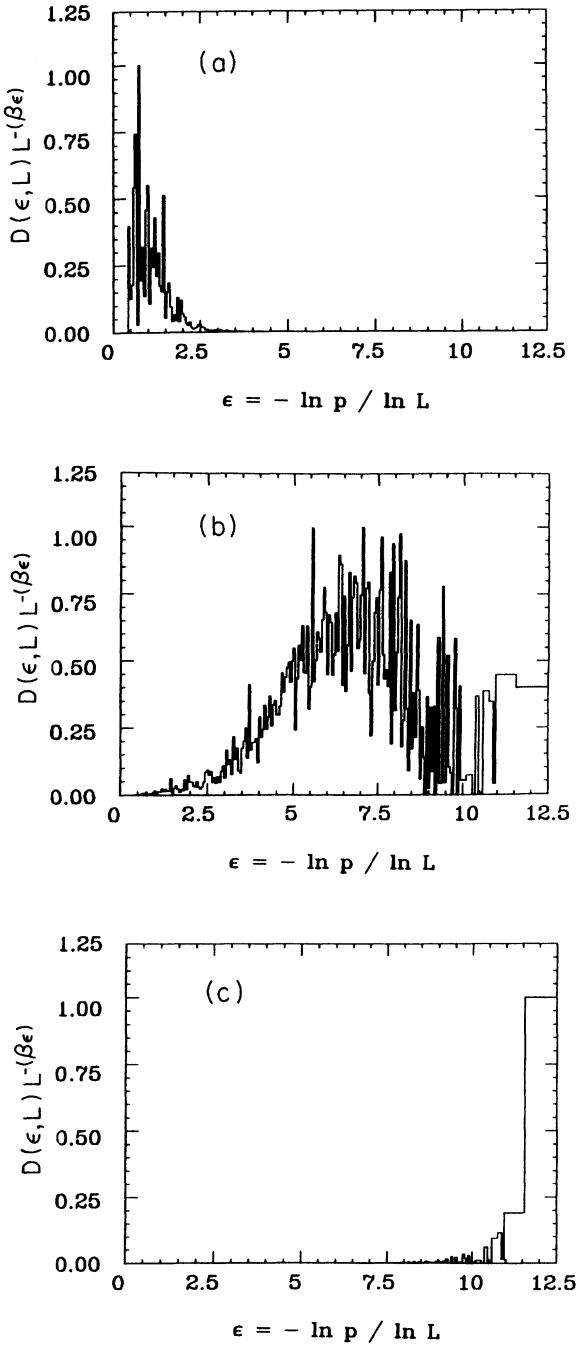

FIG. 13. Energy fluctuations above, near, and below the phase transition. Shown is the density of states multiplied by the Boltzmann factor $L^{-\beta\epsilon}$ for the case of $L = 5$ and (a) $\beta = 1.0$, (b) $\beta = -1.0$, and (c) $\beta = -2.0$.

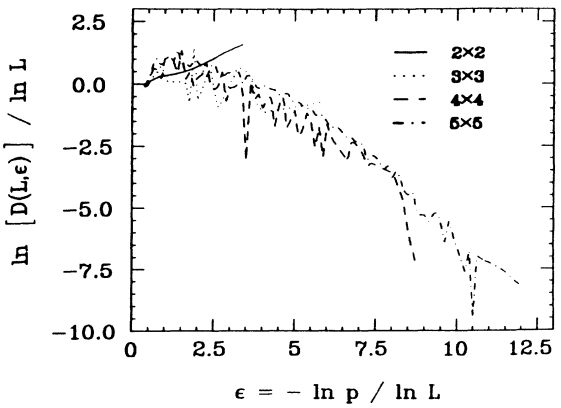

FIG. 14. Data-collapse plot showing the dependence of $\ln D(\epsilon,L)$ scaled by $\ln L$ on $-\ln P$ scaled by $\ln L$. One can see the reasonably good data collapse.

converge rapidly to $s(\epsilon^*,L)$, and become equivalent in the thermodynamic limit ($L \to \infty$). Since this assumption fails for $\beta \sim \beta_c$, the convergence of the entropy function is poor. We shall call the poor convergence of right-hand side of $S(E,L)$ "critical slowing down."

This point can be more clearly illustrated by comparing $S(E,L)$ with $s(\epsilon,L)$ obtained by a "data collapse" plot. To be more precise, consider the plot of $\ln D(\epsilon,L)/\ln L$ versus $\epsilon \equiv -\ln p/\ln L$, as shown in Fig. 14. Although the data are quite noisy, one can see a reasonably good data collapse even for the large-ϵ region. Furthermore, the $\epsilon > 5$ part of the curve is fairly linear, which also supports the existence of a phase transition.

We want to conclude this section with some comments about Monte Carlo sampling. Consider the situation that one is trying to determine the multifractal spectrum by Monte Carlo sampling. In other words, one randomly chooses one configuration out of all the possible configurations of size L, calculates the growth probabilities of that configuration by solving the Laplace equation, forms the partition function, and calculates the free energy from (4). We simulate this sampling process for $L=4$,

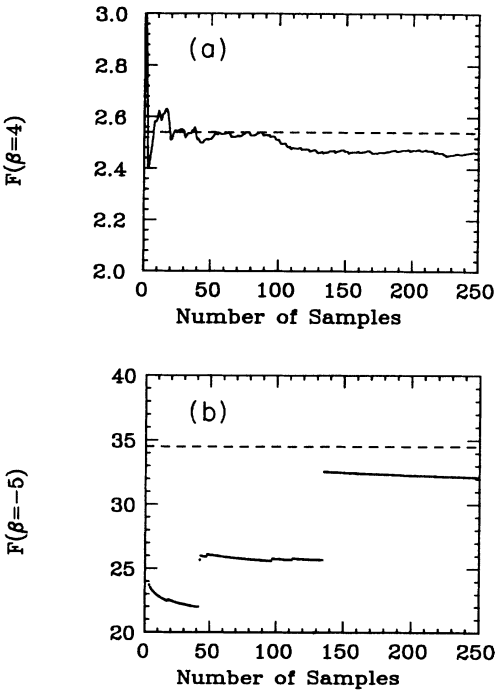

FIG. 15. Estimation of $F(\beta,L)$ by random sampling. The dashed lines are the exact value for $L=4$. (a) $\beta=4$: One can see the running average converge smoothly to the exact value. Moreover, we can get a good estimation of $F(\beta=4,L=4)$ from relatively small number of samples. (b) $\beta=-5$: The running average shows "jumps," and becomes close to the exact value after the number of samples is the same order of magnitude as the total number of configurations (259). This strange behavior is due to the sample which gives the dominant contribution to $F(\beta,L)$, but is very hard to get.

that is, at each time step, we randomly choose one out of 259 configurations proportional to their weights C_α, and calculate the free energy, as explained above. The "running average" of the free energy is determined for two values of β, as shown in Fig. 15. In contrast to the smooth convergence for the positive β, the convergence for the negative β consists of big jumps, and becomes close to the actual value after the number of samples becomes comparable to the total number of configurations.[26] This strange behavior comes from the fact that there are configurations that are very difficult to get, but that give a big contribution for the free energy. Since the free energy is dominated by these rare configurations, one should *not* expect good estimates of the multifractal spectrum for the fjord phase.

V. ORIGIN OF THE PHASE TRANSITION

In this section we discuss what *causes* the phase transition. We first argue that C_α, the weight of configuration α, as well as the growth probabilities p_i, are determined by a *multiplicative* process.

Consider clusters in a box of fixed size L. One can notice that C_α is a sum of products of some $p_{i,\alpha'}$,

$$C_\alpha = C_1 \sum_{\Gamma_\alpha} \prod_{i,\alpha'} p_{i,\alpha'} , \tag{11}$$

where Γ_α denotes all paths of configurations α' from the "initial configuration" to configuration α. Here, the initial configuration is the one which does not have any cluster bonds, whose mass is equal to the mass of the seed particles, L. If α is a configuration of mass M, all the products have $M-L$ elements, where M has a value between L and L^2. One should notice that the largest M is not equal to $2L^2-L$, the number of bonds in a box of size L, but L^2, since DLA cannot form a closed loop.

Consider now *all* possible configurations of mass M and define Γ_M as the union of all Γ_α, where configuration α has mass M. We also label the individual path, the elements of set Γ_M, with index j. Since $C_\alpha = \sum_{\Gamma_\alpha} C_j$ the partition function (3) becomes

$$Z(\beta,L) = \sum_{M=L}^{L^2} \sum_{\Gamma_M} C_j \sum_i p_{i,\alpha}^\beta , \tag{12}$$

where C_j/C_1 is a product of $M-L$ growth probabilities, and α is the final configuration on the path j. Let p_j^* denote the geometric mean of these probabilities, i.e., p^* is defined as

$$C_j = C_1 p_j^{*(M-L)} . \tag{13}$$

Next, we will argue that in order to significantly contribute to the partition function, the number of surface bonds should be order of the mass of the configuration. Compare two configurations α and γ, which have same number of surface bonds N, but have different mass M_α and M_γ. Furthermore, we assume that $M_\alpha \gg M_\gamma \simeq N$. One can notice that $C_\alpha \ll C_\gamma$, since the weights are, as shown (13), exponentially decreasing functions of M. Now, consider the sum $\Sigma \equiv \sum_i p_i^\beta$. For positive β, since

both configurations have the "tip" part, Σ for configuration α and configuration γ are about the same order of magnitude. On the other hand, since configuration α would be compact, and γ be ramified, the configuration γ has surface bonds whose p_i is very small. So, for negative β, the Σ for γ would be much larger than that for α. Therefore, the contribution to the partition function, which is the product of the weight and Σ, is dominated by configuration γ.

Consider every configuration of mass M. If N is *substantially* less than M, we can find the configuration of mass N which also has N surface bonds. From the above arguments, the contribution from this configuration of mass N and N surface bonds will be so dominant that we can ignore the configuration of mass M and N surface bonds. Therefore, we argue that only the configurations, whose number of surface bond is of the same order of the mass, are important.

To approach a further understanding of the underlying mechanism for the phase transition that gives rise to the negative-moment problem, we assume that the growth probability on the outer part of a configuration has some value $p_{\max,\alpha}$, and that the growth probability at a "depth" of i sites has a probability $p_{\max,\alpha}\hat{p}_\alpha^{\,i}$, where $\hat{p}_\alpha$ is an average penetration probability for the configuration α. We expect this assumption to be valid at least for large values of i, which is the interesting limit for the negative moments. From the considerations above we have $N_\alpha \sim M$ surface bonds for a dominant configuration of mass M. This *necessarily ramified* structure of the dominant configurations naturally leads us to a simple approach where each dominant configuration α of mass M has $M-L$ growth probabilities

$$p_{i,\alpha}=p_{\max,\alpha}\hat{p}_\alpha^{\,i} , \tag{14}$$

where $i=0,1,\ldots,M-L-1$. Since $\sum_{i=1}^{N_\alpha} p_{i,\alpha}=1$, we have

$$p_{\max,\alpha}=(1-\hat{p}_\alpha)/(1-\hat{p}_\alpha^{\,(M-L)}) . \tag{15}$$

Here we have disregarded the L growth probabilities from the original line of seed particles. Then, what is $p_{\min,L}$, the smallest growth probability among the possible configurations in a box of size L? This can be obtained by (14) with $i=M-L-1$ and $M\sim L^2$. Hence $p_{\min,L}\sim\hat{p}_\alpha^{\,L^2}$, or

$$\ln p_{\min,L}\sim L^2 , \tag{16}$$

in agreement with the numerical observation (7).

By substituting (14) in (12), the partition function becomes

$$\begin{aligned} Z(\beta,L)&=C_1\sum_{M=L}^{L^2}\sum_{\Gamma_M} p_j^{*(M-L)}p_{\max,\alpha}^{\beta}\sum_{i=0}^{M-L-1}\hat{p}_\alpha^{\,i\beta} \\ &=C_1\sum_{M=L}^{L^2}\sum_{\Gamma_M} p_j^{*(M-L)}p_{\max,\alpha}^{\beta} \\ &\quad\times(1-\hat{p}_\alpha^{\,\beta(M-L)})/(1-\hat{p}_\alpha^{\,\beta}) , \end{aligned} \tag{17}$$

for $\beta=0$, the third sum is $M-L$. One can also notice that

$$C_1\sum_{M=L}^{L^2}\sum_{\Gamma_M} p_j^{*(M-L)}=\sum_\alpha C_\alpha=1 . \tag{18}$$

We consider two cases. (i) For $\beta>0$, since $(1-\hat{p}_\alpha^{\,\beta(M-L)})/(1-\hat{p}_\alpha^{\,\beta})$ becomes number less than 1, one can notice that the last sum in (17) converges in the large-L limit for all *positive* values of β. (ii) For $\beta<0$ this is not always true. The terms which determine the convergence of the sum in (17) are the products

$$p_j^{*(M-L)}\hat{p}_\alpha^{\,\beta(M-L)}=(p_j^*\hat{p}_\alpha^{\,\beta})^{(M-L)} , \tag{19}$$

i.e.,

$$Z(\beta,L)\sim C_1\sum_{M=L}^{L^2}\sum_{\Gamma_M}(p_j^*\hat{p}_\alpha^{\,\beta})^{(M-L)} . \tag{20}$$

To reduce the sum in (20), define by $K_M(p^*,\hat{p})dp^*d\hat{p}$ the total number of paths j leading to a configuration α of mass M for which p_j^* has a value between p^* and p^*+dp^* and $\hat{p}_\alpha$ has a value between $\hat{p}$ and $\hat{p}+d\hat{p}$. By (18), $C_1K_M(p^*,\hat{p})$ cannot increase faster than exponentially, and therefore we write $C_1K_M(p^*,\hat{p})$ as $[n(p^*,\hat{p})]^{(M-L)}$. Converting the sum in (20) over the paths Γ_M into an integral over p^* and $\hat{p}$ yields

$$\begin{aligned} Z(\beta,L)&\sim\sum_{M=L}^{L^2}\int[n(p^*,\hat{p})p^*\hat{p}^{\,\beta}]^{(M-L)}dp^*d\hat{p} \\ &=\sum_{M=L}^{L^2}[n(q^*,\hat{q})q^*\hat{q}^{\,\beta}]^{(M-L)} , \end{aligned} \tag{21}$$

where q^* and $\hat{q}$ are defined by steepest descent, i.e., where $n(p^*,\hat{p})p^*\hat{p}^{\,\beta}$ is maximal.

We notice that q^* and $\hat{q}$ may depend on β; however, we expect this dependence to be *smooth*. As regards the origin of the phase transition we an therefore take q^* and $\hat{q}$ to be β independent. Then, from (21) two results are obtained: (i) At and below

$$\beta_c\equiv-\frac{\ln[n(q^*,\hat{q})q^*]}{\ln\hat{q}} , \tag{22}$$

the partition function diverges; (ii) below β_c the partition function has the form

$$Z(\beta,L)\sim p_{\min,L}^{\,a(\beta-\beta_c)} , \tag{23}$$

where a is of order 1 [in general a will be a slowly varying function of β with $a=a(\beta)$ of order 1]. Equation (23) is in perfect agreement with our numerical results, as shown in Fig. 7(b). In particular, also the free energy $F(\beta,L)$ [Eq. (4)] diverges for $\beta<\beta_c$.

Our numerical results suggest that $n(q^*,\hat{q})q^*\gtrsim\hat{q}$. Finally, our approach has not taken any nontrivial scaling behavior of the outer part of the aggregate into account. Still, the phase transition originates from an *exponential* divergence,[21(b)] and is therefore *not* influenced by power laws.

VI. CONCLUSION

We studied the multifractal spectrum of DLA using an exact enumeration approach. The enormous number of

configurations is greatly reduced by finding $2L$ symmetry operators (L translational operators and L inversion operators), and repeatedly applying these operators. By this symmetry consideration, we are able to obtain the multifractal spectrum up to $L=5$. In the multifractal spectrum, we find evidence strongly suggesting the existence of a phase transition: the free energy, energy, and specific heat develop singularities near a critical temperature β_c. This phase transition implies the following. (1) The free energy is not defined for $\beta<\beta_c$; this is commonly called the negative moment problem. (2) The large E part of the entropy function is a straight line of slope β_c. (3) There are large fluctuations of energy near the critical temperature ($\beta\simeq\beta_c$). This phase transition is of significance for several reasons.

(1) The phase transition is a natural explanation for the negative-moment problem, which has plagued the investigators in this field.

(2) The phase transition gives valuable information about the fjord area, such as the entropy function, where no reliable calculation has previously been done.

(3) The phase transition may give insights into the physics of DLA. Finally we presented a phenomenological argument to explain the origin of this phase transition.

Note added in proof. After this work was submitted for publication, we received a related preprint [R. Blumenfeld and A. Aharony (unpublished)] which supports the possibility that there is a phase transition in the multifractal spectrum of DLA, as proposed in Ref. 22 and in this work. We thank Dr. Blumenfeld and Dr. Aharony for sending us a copy of their work prior to publication.

ACKNOWLEDGMENTS

We thank M. Jensen, S. Redner, and especially A. Aharony and R. Blumenfeld for helpful feedback, and the National Science Foundation, Office of Naval Research, and Boston University Academic Computing Center for support. One of us (P.A.) also acknowledges support from the Carlsberg Foundation and the Danish Natural Science Research Council.

APPENDIX A: DETERMINATION OF σ^*

In this section, we will describe the Nagatani renormalization method used to obtain σ^*, the conductance of the surface bond. As explained in Sec. II, σ^* is due to the small structures ignored in the conventional coarse-graining process. In other words, σ^* should be calculated by considering the configurations which *do not* have a spanning cluster.

For example, let us consider the 2×2 cell. First, we find the configurations α that do not span. These configurations are precisely those used in the exact enumeration calculation (cf. Figs. 3 and 5). Then for each configuration α, we calculate the weight C_α and the conductance $\mathcal{S}_\alpha$. Both are functions of the conductance of the surface bond. Since we do not know the conductance of the surface bond, let us assign some value σ. We also define the conductance σ' as the geometrical average of conductances of all the configurations which do not span. In other words,

$$\ln\sigma' \equiv \sum_{\alpha=1}^{N} C_\alpha(\sigma)\ln\mathcal{S}_\alpha(\sigma) , \tag{A1}$$

where N is the total number of configurations.

For a 2×2 cell, one can see, from Fig. 5, $N=3$,

$$C_1=(4+3\sigma)/(11+6\sigma),\quad C_2=C_1,\quad C_3=3/(11+6\sigma) . \tag{A2}$$

Moreover, the conductances of these configurations are determined to be $\mathcal{S}_1(\sigma)=2\sigma/(1+\sigma)$, $\mathcal{S}_2(\sigma)=(4\sigma+3\sigma^2)/(1+3\sigma)$, and $\mathcal{S}_3(\sigma)=2\sigma$. The renormalization equation (A1) becomes

$$\ln\sigma'=\frac{4+3\sigma}{11+6\sigma}\ln\left[\frac{2\sigma}{1+\sigma}\right]+\frac{4+3\sigma}{11+6\sigma}\ln\left[\frac{4\sigma+3\sigma^2}{1+3\sigma}\right]+\frac{3}{11+6\sigma}\ln(2\sigma) . \tag{A3}$$

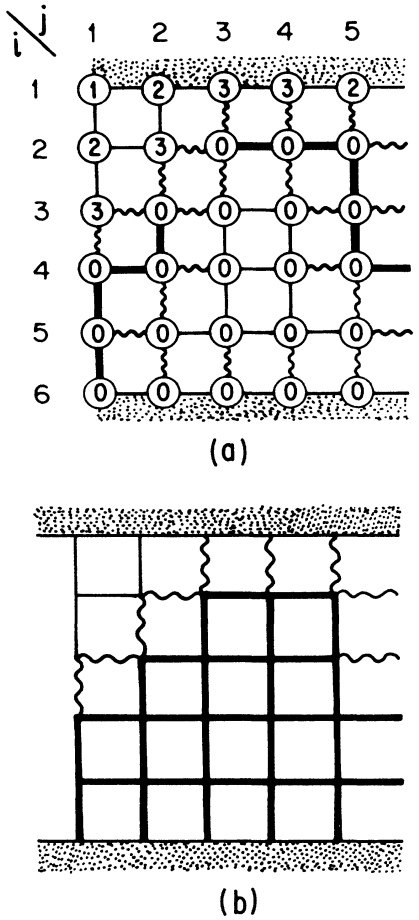

FIG. 16. Identification of zero-voltage-drop surface bonds. (a) A typical configuration with zero-voltage-drop surface bonds, and the counters on the lattice are shown. (b) The same configuration after replacing the zero-voltage-drop surface bonds with cluster bonds. One can notice the enormous reduction of the surface bonds.

We similarly obtain renormalization equations for $L=3,4,5$.

By setting $\sigma=\sigma'$, we find the stable fixed points $\sigma^*(L)$, which are 2.326, 2.193, 2.089, and 2.066 for $L=2$, 3, 4, and 5, respectively. What is the meaning of these fixed points? $\sigma^*(L)$ is the average conductance of the small structures after an infinite number of coarse graining. Thus $\sigma^*(L)$ is a good approximation of the conductance of the surface bond. For $L\times L$ exact enumeration, we used the $\sigma^*(L)$ as the conductance of a surface bond.

APPENDIX B: BURNING ALGORITHM

Consider a 5×5 cell configuration as shown in Fig. 16(a). One can see that there are many surface bonds whose voltage drops are zero. As explained in Sec. III, the identifications of these bonds and replacement with cluster bonds is very important.

The term "burning" was proposed by Herrmann *et al.*[25] to describe an algorithm in which sites are successively labeled ("burned") as in a forest fire. Burning algorithms are used to determine cluster structure, such as minimum path length, backbone mass, and blob size distribution.

The algorithm we used is a slight modification of the burning algorithm. One can specify a lattice point by indicating its row and column (i,j). For example, (1,1) is the upper-left corner and (6,5) is the lower-right corner. At each lattice point, we assign a counter (which we show as a circle). The value of each counter is set to be zero, except for the one at (1,1), which is given the value of 1. The counter indicates whether a random walker has passed the point or not. Initially the random walker is at (1,1). In the next step, the random walker checks every nearest neighbor sites and moves as follows.

(1) If the site is not on the lattice, the walker cannot move onto the site.

(2) If the site is occupied by a cluster bond or bonds, the walker cannot move onto the site.

(3) If the counter on the site is nonzero, it cannot move onto the site.

(4) If none of the above conditions (1)–(3) applies, the walker moves onto the site and sets the counter to be 2.

In the next step, we check all the nearest-neighbor sites of the counter=2 sites. We now apply the same rules (1)–(4), except we set the counter at 3 for the newly visited sites. We continue this process until all the nearest-neighbor sites are blocked. The value of the counter after the random walk is shown in Fig. 16(a).

The sites with a counter of 0 are either sites with cluster bonds or sites that cannot be reached by the random walker. So a bond with zero counters on both sides should be one of three following cases.

(1) Both sides are occupied with cluster bonds. Obviously no voltage drop is applied to this bond.

(2) Both sites are not-visited sites. If we consider the random walker as an electron, this means that there is no current through this bond, implying a zero-voltage drop.

(3) One site is a not-visited site and the other is a site with a cluster. By the same logic as (2), there is no voltage drop across this bond.

Therefore we can identify the bonds with zero counters on both sides as the bonds with zero-voltage drop. Since there is no voltage drop across these bonds, we can replace it with cluster bonds [see Fig. 16(b)]. As shown in this example, this identification plays a very important role in reducing daughter structures, from 25 to 9 in this example.

[1]T. A. Witten and L. Sander, Phys. Rev. Lett. **47**, 1400 (1981); Phys. Rev. B **27**, 5686 (1983).

[2]Applications are described in many recent review articles. See, e.g., P. Meakin, in *Phase Transitions and Critical Phenomena,* edited by C. Domb and J. L. Lebowitz (Academic, Orlando, 1988), Vol. 12.

[3]For general background, see the recent books, (a) J. Feder, *Fractals* (Pergamon, New York, 1988); (b) *Random Fluctuations and Pattern Growth: Experiments and Models,* edited by H. E. Stanley and N. Ostrowsky (Kluwer Academic, Dordrecht, 1988); (c) T. Vicsek, *Fractal Growth Phenomena* (World Scientific, Singapore, 1989), and references therein.

[4]T. C. Halsey, P. Meakin, and I. Procaccia, Phys. Rev. Lett. **56**, 854 (1986).

[5]C. Amitrano, A. Coniglio, and F. di Liberto, Phys. Rev. Lett. **57**, 1016 (1986).

[6]P. Meakin, H. E. Stanley, A. Coniglio, and T. A. Witten, Phys. Rev. A **32**, 2364 (1985); P. Meakin, A. Coniglio, H. E. Stanley, and T. A. Witten, *ibid.* **34**, 3325 (1985); A. Coniglio, in *On Growth and Form: Fractal and Non-Fractal Patterns in Physics,* edited by H. E. Stanley and N. Ostrowsky (Nijhoff, Dordrecht, 1985), p. 101; in *Fractals in Physics,* edited by L. Pietronero and E. Tosatti (North-Holland, Amsterdam, 1986); Physica A **140**, 51 (1986).

[7]B. B. Mandelbrot, J. Fluid Mech. **62**, 331 (1974). See also the recent review, B. B. Mandelbrot, in *Random Fluctuations and Pattern Growth: Experiments and Models,* edited by H. E. Stanley and N. Ostrowsky (Kluwer Academic, Dordrecht, 1988).

[8]H. G. E. Hentschel and I. Procaccia, Physica **8D**, 435 (1983); P. Grassberger, Phys. Lett. A **97**, 277 (1983); D. Schertzer and S. Lovejoy, in IUTAM Symposium on Turbulence and Chaotic Phenomena in Fluids, Kyoto, Japan, 1983 (unpublished), p. 141; P. Grassberger and I. Procaccia, Physica **13D**, 34 (1984); P. Grassberger, Phys. Lett. **107A**, 101 (1985); R. Benzi, G. Paladin, G. Parisi, and A. Vulpiani, J. Phys. A **17**, 3521 (1984); **18**, 2157 (1985); U. Frisch and G. Parisi, in *Turbulence and Predictability in Geophysical Fluid Dynamics and Climate Dynamics,* Proceedings of the International School of Physics "Enrico Fermi," Course LXXXVIII, edited by M. Ghil, R. Benzi, and G. Parisi (North-Holland, Amsterdam, 1985); S. Lovejoy and D. Schertzer, Bull. Am. Met. Soc. **67**, 221 (1986); S. Lovejoy, D. Schertzer, and A. A. Tsonis, Science **231**, 1036 (1987).

[9]T. C. Halsey, M. H. Jensen, L. P. Kadanoff, I. Procaccia, and B. I. Shraimann, Phys. Rev. A **33**, 1141 (1986).

[10]H. Gould, F. Family, and H. E. Stanley, Phys. Rev. Lett. **50**, 686 (1983).

[11]R. C. Ball, R. M. Brady, G. Rossi, and B. R. Thompson, Phys. Rev. Lett. **55**, 1406 (1985).

[12]G. Parisi and Y. C. Zhang, J. Stat. Phys. **41**, 1 (1985).

[13]Y. Hayakawa, S. Sato, and M. Matsushita, Phys. Rev. A **36**, 1963 (1987).

[14]T. C. Halsey, Phys. Rev. Lett. **59**, 2067 (1987).

[15]I. Procaccia and R. Zeitak, Phys. Rev. Lett. **60**, 2511 (1988).

[16]T. Bohr, P. Cvitanović, and M. H. Jensen, Europhys. Lett. **6**, 445 (1988).

[17]L. Pietronero, A. Erzan, and C. Evertsz, Phys. Rev. Lett. **61**, 861 (1988).

[18]See, e.g., the discussion on this point in K. J. Måløy, F. Boger, J. Feder, and T. Jøssang, in *Time Dependent Effects in Disordered Materials,* edtied by R. Pynn and T. Riste (Plenum, New York, 1987); J. Nittmann, H. E. Stanley, E. Touboul, and G. Daccord, Phys. Rev. Lett. **58**, 619 (1987); P. Alstrøm, Phys. Rev. A **37**, 1378 (1988).

[19]T. Nagatani, Phys. Rev. A **36**, 5812 (1987); J. Phys. A **20**, L381 (1987).

[20]The concept of a phase transition in multifractal spectra was found in the study of dynamical systems, such as the logistic map [T. Bohr and M. Jensen, Phys. Rev. A **36**, 4904 (1987); M. Duoung-van, Nucl. Phys. B (Proc. Suppl.) **2**, 521 (1987)], Julia Sets [D. Katzen and I. Procaccia, Phys. Rev. Lett. **58**, 119 (1987); M. Jensen, P. Cvitanović, and T. Bohr, Europhys. Lett. **6**, 445 (1988)]. See also R. Artuso, P. Cvitanović, and B. Kenney, Phys. Rev. A **39**, 277 (1989); P. Cvitanović, in *XV International Colloquium on Group Theoretical Methods in Physics,* edited by R. Gilmore (World Scientific, Singapore, 1987); D. Katzen and I. Procaccia, Phys. Rev. Lett. **58**, 1169 (1987); R. Badii and A. Politi, Phys. Scr. **35**, 243 (1987); P. Grassberger, R. Badii, and A. Politi, J. Stat. Phys. (to be published); P. Szépfalusy, T. Tél, A. Csordas, and Z. Kovacs, Phys. Rev. A **36**, 3252 (1987); M. J. Feigenbaum, J. Stat. Phys. **52**, 527 (1988); R. Artuso, J. Phys. A **21**, L923 (1988). In particular, based on a study of Julia sets, Bohr *et al.* conjectured the existence of a phase transition for aggregates generated by probabilistic diffusion. This conjecture has been supported further from a description of stochastic growth phenomena as a dynamical critical state [see, e.g., P. Alstrøm (unpublished); P. Alstrøm, P. Trunfio, and H. E. Stanley in Ref. 3(b)]. However, the present work presents the first direct evidence for a phase transition in a *realistic* model system.

[21](a) Regarding the moments of the distribution of voltage drops across the bonds of a random resistor network, L. de Arcangelis, S. Redner, and A. Coniglio [Phys. Rev. B **34**, 4656 (1986)] observed a change in the relative importance of the contribution of the hottest and coldest bonds to the moments, suggesting the possibility of a transition point. (b) R. Blumenfeld, Y. Meir, A. Aharony, and A. B. Harris [Phys. Rev. B **35**, 3524 (1987)] carried out exact low concentration expansions for the random resistor network, calculating exactly the negative moments for all configurations of small clusters (up to 11 bonds) on a square lattice. Moreover, they proved for a "ladder model" of the random resistor network that exponentially small currents appear, leading to a transition where the multifractal description breaks down and the moments diverge. (c) A phase transition has also been observed for the voltage drops across the bonds of the Sierpinski gasket family of deterministic fractals [P. Alstrøm, D. Stassinopoulos, and H. E. Stanley, Physica A **153**, 20 (1988)], which very recently has been shown to hold more generally in resistor networks and dynamical systems that have a renormalizable matrix structure for the distribution in question. [P. Alstrøm, D. Stassinopoulos, and H. E. Stanley (unpublished)].

[22]This work is a more complete report of recent exact results in Phys. Rev. Lett. **61**, 2945 (1988).

[23]L. Niemeyer, L. Pietronero, and H. J. Wiesmann, Phys. Rev. Lett. **52**, 1033 (1984).

[24]D. Ruelle, *Statistical Mechanics, Thermodynamic Formalism* (Addison-Wesley, Reading, MA, 1975); M. J. Feigenbaum, J. Stat. Phys. **46**, 919 (1987); **46**, 925 (1987); T. Bohr and D. Rand, Physica D **25**, 387 (1987).

[25]H. J. Herrmann, D. C. Hong, and H. E. Stanley, J. Phys. A **17**, L261 (1984).

[26]Similar problems in random sampling process are described in H. E. Stanley and P. Meakin, Nature **335**, 405 (1988); S. Redner, Am. J. Phys. (to be published); S. Havlin, R. Blumberg Selinger, M. Schwartz, H. E. Stanley, and A. Bunde, Phys. Rev. Lett. **61**, 1438 (1988).